Research Article Open Access

Lei Wu and Yong Zhang*

Enhanced thermal oxidative stability of silicone rubber by using cerium-ferric complex oxide as thermal oxidative stabilizer

https://doi.org/10.1515/epoly-2019-0026
Received November 07, 2018; accepted December 13, 2018.

Abstract: Cerium (Ce)-ferric (Fe) complex oxides were prepared via a citric acid sol-gel process, and used as thermal oxidative stabilizers for silicone rubber (SR). The oxides were characterized by X-ray diffraction and Raman spectroscopy. The Ce/Fe molar ratio in Ce-Fe complex oxides significantly influenced the thermal oxidative stability of SR. After aging at 300°C for 24 h, SR filled with 4 phr Ce-Fe complex oxide with a Ce/(Ce+Fe) molar ratio of 0.8 (CeFeO-0.8) exhibited excellent thermal oxidative stability, retaining 56.8% and 54.3% of its original tensile strength and elongation at break, respectively. Some Ce^{3+} and Fe^{2+} ions were detected in aged SR composites. Ce^{3+}/Ce^{4+} and Fe^{2+}/Fe^{3+} molar ratios in SR/CeFeO-0.8 were less than that in SR/CeO_2 and SR/Fe_2O_3 composites, respectively, as detected by X-ray photoelectron spectroscopy. It implies rapid re-oxidations of Fe^{2+} and Ce^{3+} occurred in SR/CeFeO-0.8, enhancing the capacity of CeFeO-0.8 to capture radicals during thermal aging.

Keywords: Ce-Fe complex oxide; silicone rubber; thermal oxidative stability; radical; thermal aging

1 Introduction

Silicone rubber (SR) has attracted great attention for its high thermal oxidative stability, which can maintain good performance at 250°C for a long time. However, with the advancement of frontier technologies, SR is expected to be used at higher temperature in practical applications. Two competing mechanisms were proposed for describing the degradation process of SR under the presence of heat and oxygen (1-4). The first is the molecular mechanism that occurs with the depolymerization of SR backbone and the formation of cyclic oligomers, which can shorten the length of SR macromolecule chains, consequently leading to the decreasing of crosslink density. The second is the radical mechanism that functions in side chains of SR under oxygen atmosphere where crosslinking reactions take place, causing the increase of crosslink density.

Some thermal resistant additives were used to improve the thermal oxidative stability of SR, e.g., metal oxides (5-10), carbon nanotubes (CNTs) (11-13), graphene (14) and polyhedral oligomeric silsesquioxanes (POSS) (15, 16). Among the additives, rare earth oxides and transition metal oxides such as CeO_2 and Fe_2O_3 have been widely used. SR filled with CeO_2 retained 67% and 62% of its original tensile strength and elongation at break, respectively, when subjected to thermal aging at 250°C for 3 days (6). Ce^{4+} or Fe^{3+} ions capture radicals and thus suppress the degradation of SR, which is a well-known antioxidation effect mechanism of metal oxides. A new mechanism was proposed for the antioxidation effect of α-Fe_2O_3 for SR at elevated temperature. The redox cycle of Fe^{3+} occurs on the outer part of SR but α-Fe_2O_3 reverts into the form of Fe_3O_4 in the inner layer of SR (8). The synergistic effects of two fillers were also studied. Fe_2O_3 modified CNTs was more efficient than Fe_2O_3 for improving the thermal oxidative stability of SR, which was attributed to that CNTs could facilitate the shift from α-Fe_2O_3 to γ-Fe_2O_3 which is a better stabilizer, and the electron transportation effect of CNTs on Fe_2O_3 (8-10,17). CNTs and SnO_2 nanoparticles also exhibited a positive synergistic effect on the thermal oxidative stability of SR (12).

Ce-Fe complex oxides were developed for heterogeneous catalysts. The incorporation of a small amount of Fe_2O_3 into CeO_2 can enhance the redox properties and lattice oxygen mobility of CeO_2 by lowering the activation energy of oxygen migration, thus improving

* **Corresponding author: Yong Zhang,** School of Chemistry and Chemical Engineering, State Key Laboratory for Metal Matrix Composite Materials, Shanghai Jiao Tong University, Shanghai 200240, PR China, e-mail: yong_zhang@sjtu.edu.cn, Tel: +86-21-54743261.
Lei Wu, School of Chemistry and Chemical Engineering, State Key Laboratory for Metal Matrix Composite Materials, Shanghai Jiao Tong University, Shanghai 200240, PR China.

the catalytic properties of CeO_2 (18-21). However, to our knowledge, Ce-Fe complex oxides have not been reported as thermal stabilizers for SR. In this article, Ce-Fe complex oxides were prepared by a citric acid sol-gel method, and were modified with phenyltriethoxysilane to avoid the their aggregation in SR. Ce-Fe complex oxides were then mixed into SR to investigate their effect as thermal oxidative stabilizers.

2 Experimental

2.1 Materials

$Ce(NO_3)_3{\cdot}6H_2O$, $Fe(NO_3)_3{\cdot}9H_2O$, phenyltriethoxysilane and $NH_3{\cdot}H_2O$ were purchased from Shanghai Macklin Biochemical Co., Ltd. Citric acid and ethylene glycol were purchased from Shanghai Lingfeng Chemical Reagent Co., Ltd. Polymethylvinylsiloxane (PMVS)/silica compound (denoted as SR, 100 phr silicone rubber gum (Mn = 5.9×10^4, vinyl content: 0.26 wt%) filled with 50 phr silica and additives) and 2,5-dimethyl-2,5-di-(tert-butylperoxy) hexane (DBPMH) were supplied by Midgold Fine Performance Materials (Shenzhen) Co., Ltd.

2.2 Preparation of thermal oxidative stabilizer

CeO_2, Fe_2O_3 and Ce-Fe complex oxide (CeFeO) were synthesized via the citric acid sol-gel method by referring to the literature (22). $Ce(NO_3)_3{\cdot}6H_2O$ and $Fe(NO_3)_3{\cdot}9H_2O$ were dissolved in water according to the molar ratio in Table 1. Citric acid and ethylene glycol were then added slowly into the mixed solution (the molar ratio of citric acid /ethylene glycol/total metal ions was 1.5:1:1). The pH value of the solution was adjusted to 10-11 by adding $NH_3{\cdot}H_2O$. The solution was kept in a water bath at 80°C until the gelation was completed. The as-prepared gel was then dried at 120°C for 24 h, followed by heating to 500°C at a heating rate of 5°C/min and kept for 4 h to obtain Ce-Fe complex oxide. A simple mixture of CeO_2 and Fe_2O_3 with a Ce/(Ce+Fe) molar ratio of 0.8 (denoted as CeO_2/Fe_2O_3) was prepared as a reference by directly grinding CeO_2 and Fe_2O_3 together.

2.3 Surface modification of thermal oxidative stabilizer

1 g thermal oxidative stabilizer, 0.1 g phenyltriethoxysilane (PTES) and 20 mL ethanol were mixed under ultrasonication for 30 min and stirred at 60°C for 6 h. The resultant mixture was centrifugated, and the precipitate was washed with ethanol for three times and dried in a vacuum oven at 60°C to obtain modified oxides (m-CeO_2, m-Fe_2O_3, m-CeFeO and m-CeO_2/Fe_2O_3).

Table 1: The formula of CeO_2, Fe_2O_3 and CeFeO.

Sample	$Ce(NO_3)_3$:$Fe(NO_3)_3$ (molar ratio)	Ce/(Ce+Fe) molar ratio
CeO_2	1:0	1
CeFeO-0.8	4:1	0.8
CeFeO-0.6	3:2	0.6
CeFeO-0.4	2:3	0.4
CeFeO-0.2	1:4	0.2
Fe_2O_3	0:1	-

2.4 Preparation of SR composites

150 phr PMVS/silica compound, 4 phr modified or unmodified stabilizer and 2 phr DBPMH were mixed on a two-roll mill. The obtained compound was then cured at 170°C under a pressure of 10 MPa for the optimum curing time t_{90}. SR filled with 4 phr m-CeO_2/Fe_2O_3 was prepared as a reference. The fabrication process of SR composites was illustrated in Figure 1.

2.5 Thermal oxidative aging

The vulcanizates were aged in an air-blowing oven at 300°C for 24 h.

2.6 Characterization and measurement

X-ray diffraction (XRD) patterns were measured on a Bruker D8 Advance using Cu Kα radiation (λ = 1.54 Å). Raman spectra were obtained by using a DXR Raman spectrometer with 532 nm laser excitation. The morphology of thermal oxidative stabilizer was observed by transmission electron microscopy (TEM, JEOL2100F). And Scanning electron microscope (SEM) images and energy dispersive spectroscopy (EDS) were obtained on a Hitachi S-2150 field-emission SEM system. Fourier transform infrared (FTIR) spectra were obtained on a Perkin Elmer Paragon 1000PC spectrometer as the background from 500-4000 cm^{-1}. X-ray photoelectron spectroscopy (XPS) measurements were performed on an RBD upgraded PHI-5000C ESCA system (Perkin Elmer)

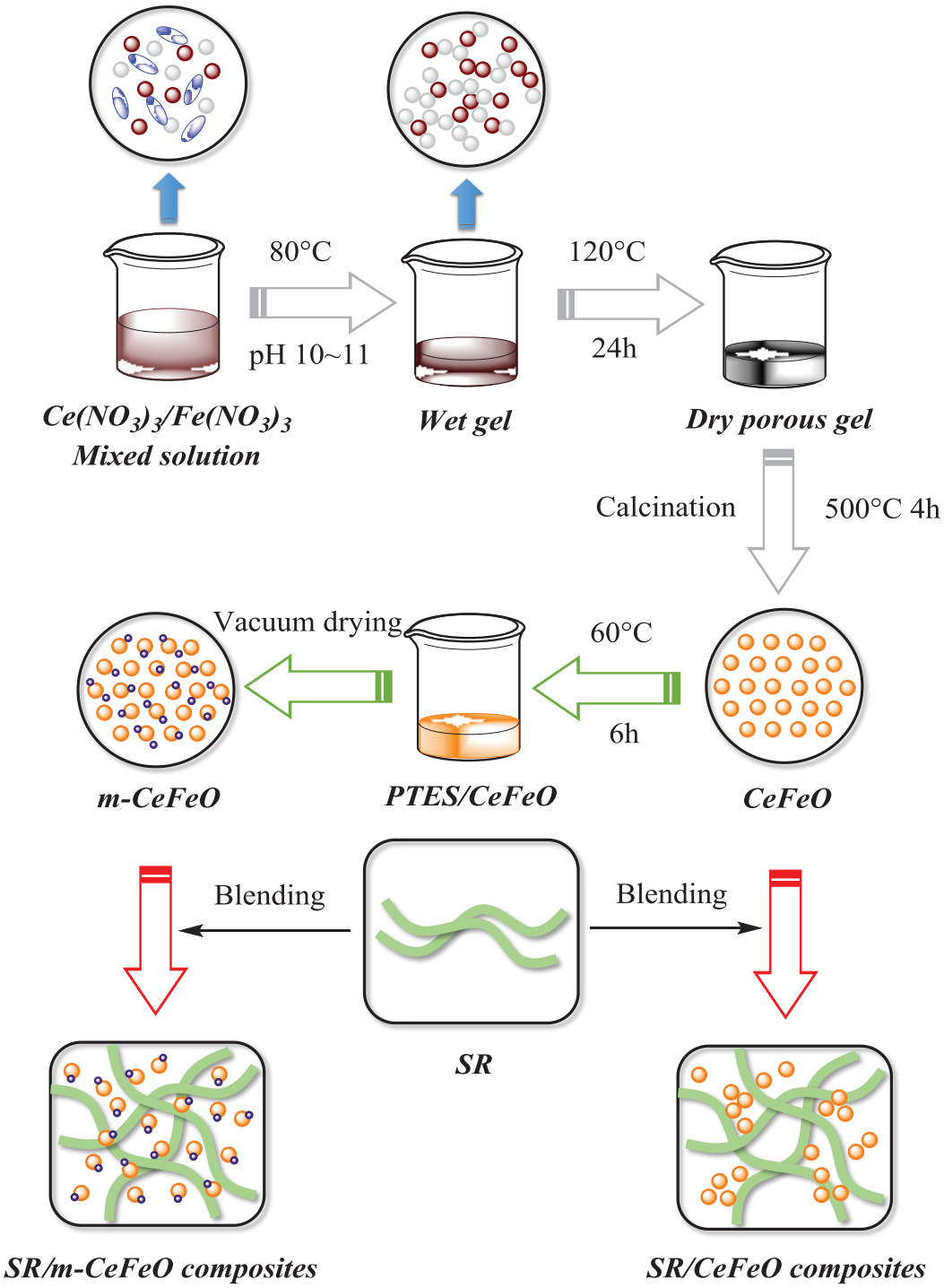

Figure 1: The fabrication process of SR composites.

with Al $K\alpha$ radiation ($h\upsilon$ = 1486 eV). To eliminate the influence of Ce^{3+} and Fe^{2+} produced during the vulcanization and improve the signal intensity of Ce3d and Fe2p XPS spectra, 100 phr silicone rubber gum was filled with 30 phr stabilizer, and the resultant compound was aged at 300°C for 48 h. The non-aged and aged samples were used for XPS measurement. The thermal stability was measured through thermogravimetric analysis (TGA) in air atmosphere at a heating rate of 20°C·min^{-1} from 50 to 700°C by using a TA Instruments Q5000IR. Stress-strain curves were obtained using a tensile machine (Instron 4465, USA) at a crosshead speed of 500 mm/min at room temperature. The crosslink density of SR vulcanizates was evaluated via the equilibrium swelling method.

The details of the process and calculation are given in the Supplementary material.

3 Results and discussion

3.1 Characterization of thermal oxidative stabilizer

XRD patterns and Raman spectra of CeO_2, Fe_2O_3 and CeFeO are shown in Figure 2. All the reflections observed in Figure 2a can be assigned to either α-Fe_2O_3 (hexagonal) (23) or cubic CeO_2 (fluorite structure) (24). For CeFeO-0.8 and CeFeO-0.6, only reflections from cubic CeO_2 are visible, while the simply mixture CeO_2/Fe_2O_3 shows the reflections of both cubic CeO_2 and α-Fe_2O_3. In the patterns of CeFeO-0.4 and CeFeO-0.2, reflections are less visible, indicating their amorphous structures which could be related to the high Fe content. Compared with pure CeO_2 and Fe_2O_3, the CeO_2 and α-Fe_2O_3 components in the CeFeO complex oxides exhibits wider and weaker diffraction peaks, which may be attributed to the reduction of crystallite size of CeO_2 and Fe_2O_3, as caused by the combination of CeO_2 and Fe_2O_3. The unit cell parameters (a) and crystalline sizes were calculated on the basis of three intensive XRD peaks (111), (220) and (311), and shown in Table 2. The unit cell parameters of cubic CeO_2 in CeFeO-0.8 (5.398 Å) and CeFeO-0.6 (5.404 Å) were a little smaller than that of pure CeO_2 (5.411 Å), suggesting that Fe^{3+} has been incorporated into the CeO_2 lattice to form a Ce-Fe solid solution, with the contraction of the cell parameter (19,25). CeFeO-0.4 and CeFeO-0.2 had considerable weak intensity of diffraction peaks in XRD patterns, and their unit cell parameter and crystalline size are unable to be calculated.

Figure 2b shows the Raman spectra of CeO_2, Fe_2O_3 and CeFeO. In the spectra of the CeFeO-0.4 and CeFeO-0.2, signals from both α-Fe_2O_3 and cubic CeO_2 are visible. In the case of the CeFeO-0.8 and CeFeO-0.6, although the Raman spectra for the complex oxides resemble that of pure CeO_2, several features should be highlighted. First, the main Raman band (I_{main}) shifted to lower frequency (454 cm^{-1} and 449 cm^{-1}, respectively) with respect to that of pure cubic CeO_2 (461 cm^{-1}), which can be ascribed to the decrease in the crystal particle size, resulting in a shift to lower frequency (19). Moreover, a weak and broad band at 598 cm^{-1} can be observed in the Raman spectra of CeFeO-0.8 and CeFeO-0.6, which is proved to be related to the oxygen vacancies in CeO_2 and also a strong

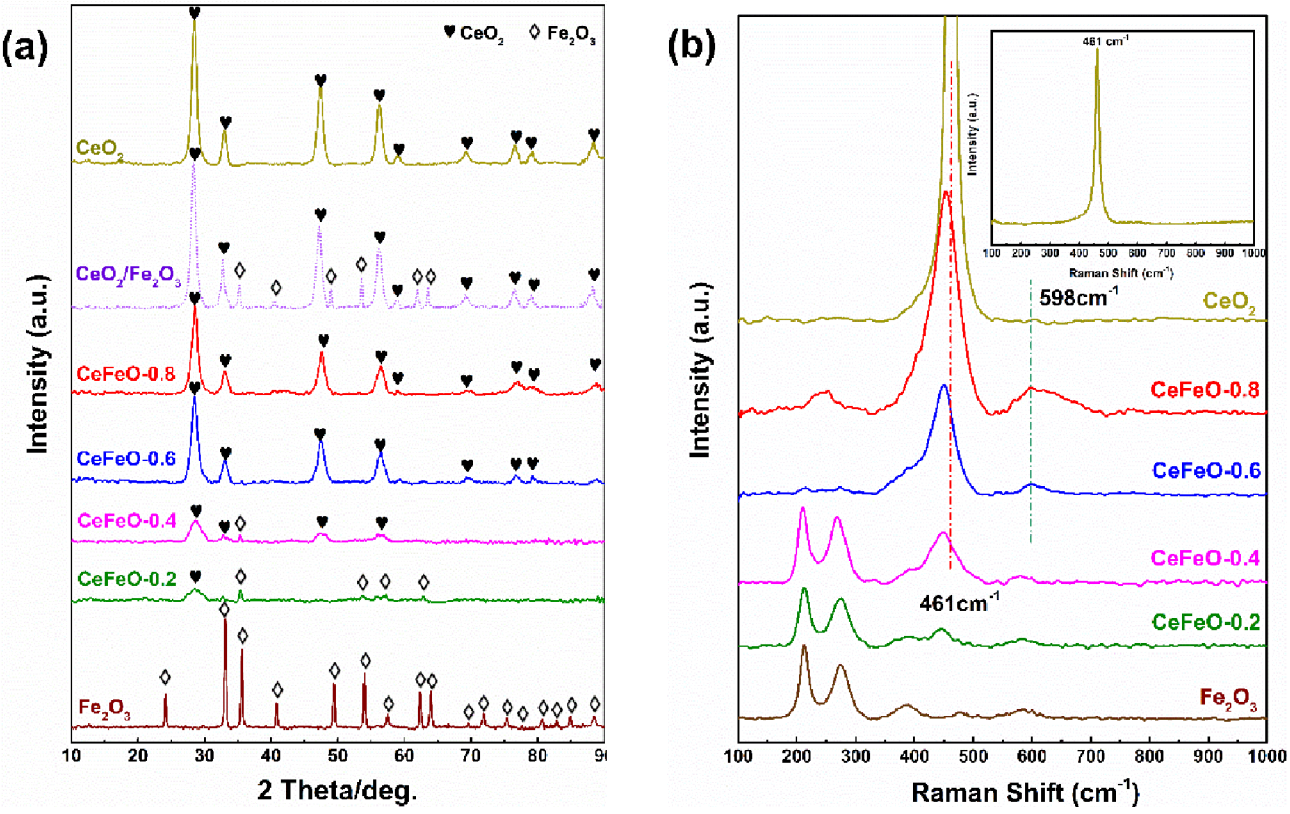

Figure 2: (a) XRD patterns and (b) Raman spectra of CeFeO. The inset in (b) is the Raman spectrum of pure CeO_2 with a characteristic peak at 461 cm^{-1}.

evidence for the formation of Ce-Fe solid solution (26). The intensity ratio of the band at 598 cm^{-1} and the main Raman band (I_{598}/I_{main}) was used to estimate the concentration of oxygen vacancies in complex oxides (20). As calculated, I_{598}/I_{main} value for CeFeO-0.8 is 0.11 which is higher than that for CeFeO-0.6 (0.09), suggesting there are more oxygen vacancies in CeFeO-0.8.

The morphology of CeFeO is shown in Figure 3. The particle sizes of CeFeO-0.8 and CeFeO-0.6 are about 10 nm, which are close to the crystalline sizes calculated from XRD. Besides, CeFeO-0.8 has slightly larger particle size than CeFeO-0.6.

3.2 Effect of PTES on the properties of thermal oxidative stabilizers and SR composites

The successful modification of the CeFeO-0.8 by PETS proved by FTIR in Figure S1. And the SEM images in Figure S2 present the positive role PTES plays in the dispersion of CeFeO-0.8 in silicone rubber (Supplementary material).

Table 2: The unit cell parameters (*a*) and crystalline sizes of CeO_2 and CeFeOs.

Sample	Unit cell parameter, a(Å)	Crystalline size (nm)
CeO_2	5.411	11.5
CeFeO-0.8	5.398	9.8
CeFeO-0.6	5.404	8.4

Figure 4 exhibits the modification effect of PTES on the mechanical properties of the SR composites. After modification, the simultaneous increases in the tensile strength and elongation at break of SR can be attributed to the more uniform distribution of CeFeO-0.8 in SR matrix, which is observed in SEM images (Figure S2). Also, the better dispersion of metal oxide particles in SR could be beneficial to the thermal oxidative stability of silicone rubber, which might be associated with the larger specific surface area so caused.

3.3 Thermal-oxidative aging properties of SR composites

The mechanical properties of SR composites before and after aging are shown in Figure 5 and Table 3. SR without any thermal oxidative stabilizer showed a cracked and shrunken appearance with a sharp rise in hardness and failed the tensile properties tests after thermal oxidative aging, indicating the occurrence of radical mechanism during thermal oxidative degradation. With the incorporation of m-CeFeO, the mechanical properties of aged SR composites could be kept to a great extent. However, the anti-oxidative performance of m-CeFeO depended on Ce/Fe mole ratio. For the aged SR/m-CeFeO-0.8 composite, the retentions of the tensile strength and elongation at break achieved 56.8% and 54.3%, respectively, which are the highest among all the composites. m-CeFeO-0.6 behaved better than

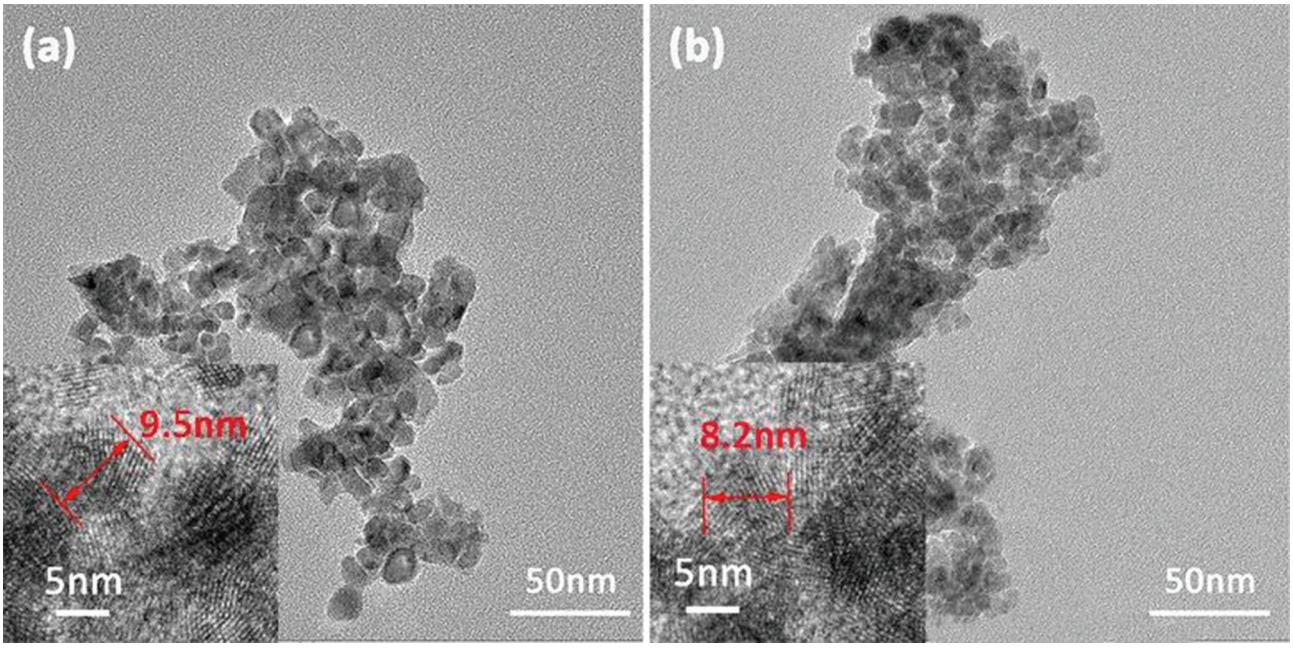

Figure 3: TEM images of CeFeO: (a) CeFeO-0.8; (b) CeFeO-0.6.

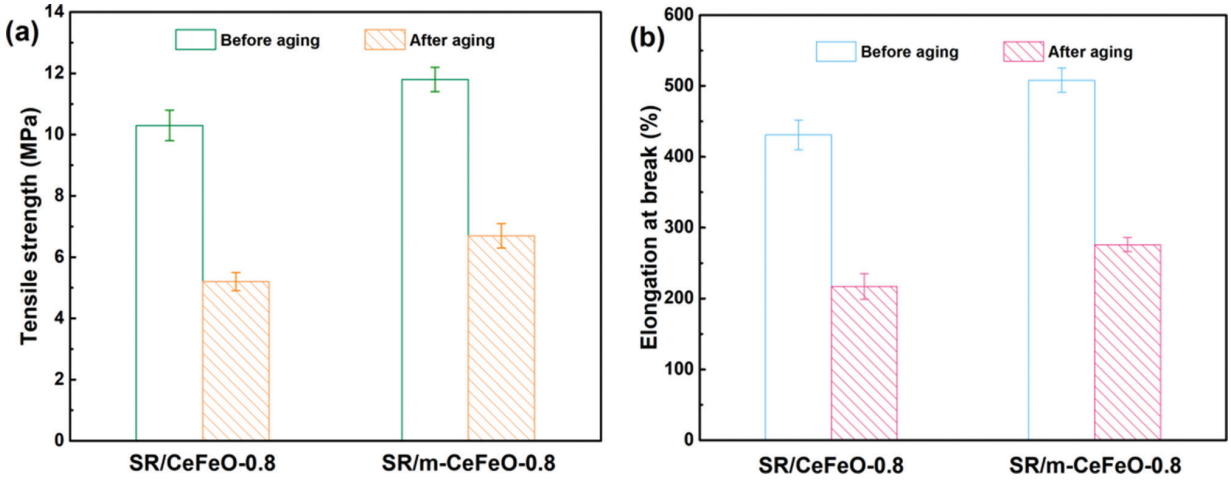

Figure 4: Mechanical properties of SR/CeFeO-0.8 and SR/m-CeFeO-0.8 composites before and after thermal oxidative aging: (a) Tensile strength; (b) Elongation at break.

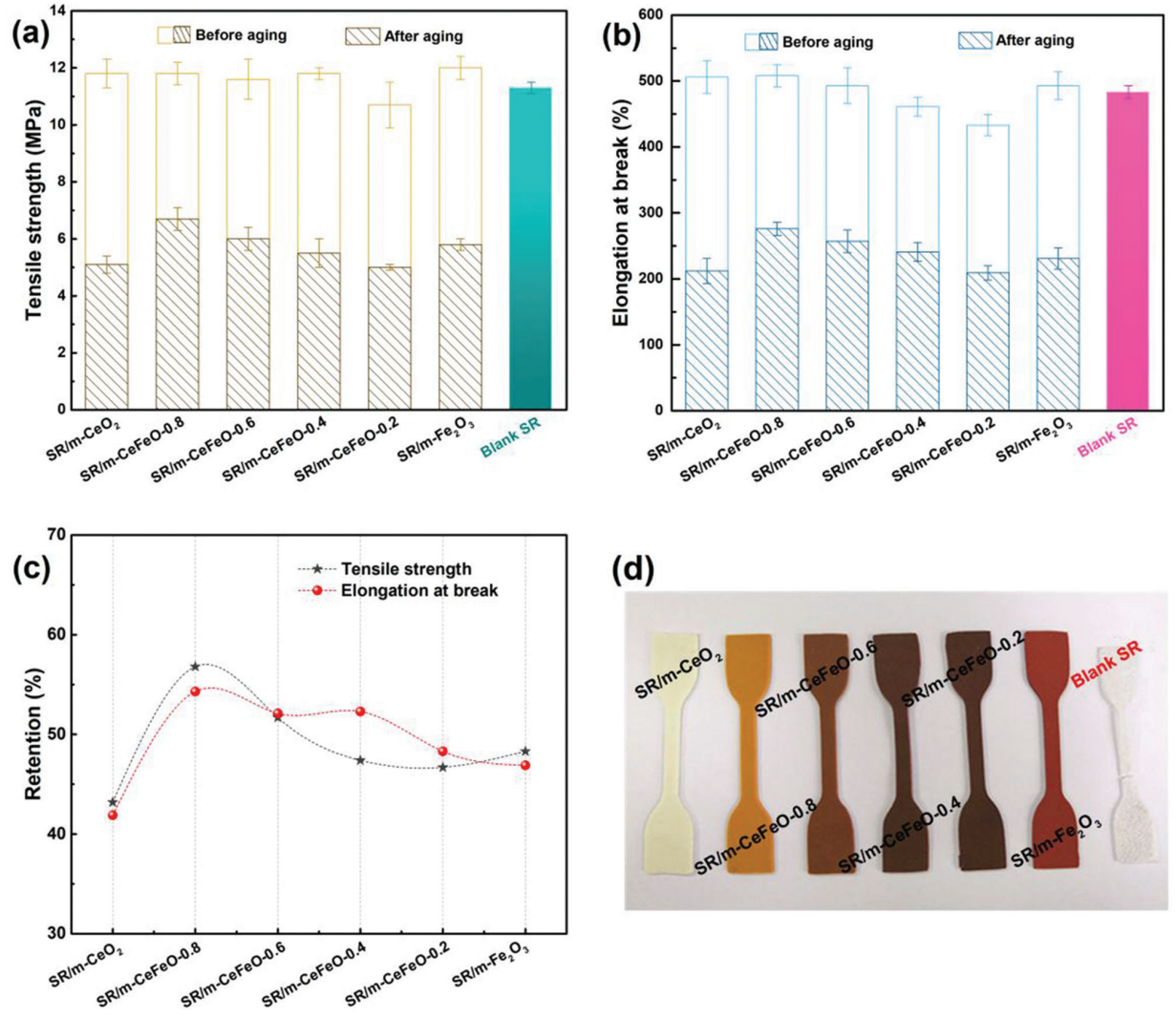

Figure 5: Mechanical properties of SR composites before and after thermal oxidative aging: (a) tensile strength; (b) elongation at break; (c) retentions of tensile strength and elongation at break (d) the photograph of SR composites after aging.

Table 3: Hardness of SR composites before and after aging.

Sample	Hardness (Shore A)	
	Before aging	After aging
SR/m-CeO_2	57.5 ± 0.5	55.3 ± 0.7
SR/m-CeFeO-0.8	57.5 ± 0.4	55.9 ± 0.4
SR/m-CeFeO-0.6	58.1 ± 0.5	56.1 ± 0.4
SR/m-CeFeO-0.4	57.7 ± 0.7	55.7 ± 0.5
SR/m-CeFeO-0.2	58.7 ± 0.4	56.7 ± 0.3
SR/m-Fe_2O_3	58.3 ± 0.6	56.3 ± 0.5
Blank SR	57.3 ± 0.6	96.4 ± 0.6

Table 4: M_c of SR composites before and after thermal oxidative aging.

Sample	$M_c \times 10^{-3}$		*Decreasing amplitude/%
	Before aging	After aging	
SR/m-CeO_2	3.48	2.80	19.5
SR/m-CeFeO-0.8	3.50	3.18	9.1
SR/m-CeFeO-0.6	3.52	3.10	12.0
SR/m-CeFeO-0.4	3.32	2.72	18.1
SR/m-CeFeO-0.2	3.41	2.76	19.1
SR/m-Fe_2O_3	3.35	2.88	14.0

m-CeO_2 and m-Fe_2O_3 in improving the thermal oxidative stability of silicone rubber. This could be ascribed to the high oxygen vacancies content caused by the incorporation of Fe^{3+} into CeO_2 lattice. Previous study showed that small doping amount of Fe^{3+} into CeO_2 facilitated the formation of oxygen vacancies whereas large doping amount of Fe^{3+} annihilated oxygen vacancies (20). Our Raman results demonstrate that there are little oxygen vacancies in CeFeO-0.4 and CeFeO-0.2 samples. The oxygen vacancies existed in CeFeO-0.8 and CeFeO-0.6 could enhance the radical capturing ability of the complex oxides, which benefits the thermal stability of SR.

3.4 The measurement of the average molecular weight between crosslinking knots (M_c) of SR composites

Swelling measurements were carried out to further explore the effect of CeFeO on the thermal-oxidative stability of SR. The changing amplitude of M_c of SR before and after aging is calculated by Eq. 1:

$$\text{Decreasing amplitude} = \frac{M_C(\text{Before aging}) - M_C(\text{After aging})}{M_C(\text{Before aging})} \quad (1)$$

The different decreasing amplitudes in M_c of SR composites before and after aging can give an indirect indication for their thermal stability and degradation mechanism. As shown in Table 4, the M_c of SR composites decreased after thermal aging under air atmosphere, which confirms it is the radical mechanism that mainly occurs during degradation process of SR under the experimental conditions of thermal aging. Focusing on the M_c decreasing amplitudes before and after aging, it is observed that the minimum variation of M_c can be achieved by SR/m-CeFeO-0.8 composite, while SR/m-CeO_2 performed worst among all SR composites. It is obvious that m-CeFeO-0.8 and m-CeFeO-0.6 function better on the thermal resistance of SR compared with pure m-CeO_2 and m-Fe_2O_3. This can be ascribed to the successful combination of CeO_2 and Fe_2O_3 in both complex oxides where oxygen vacancies have their share on the oxygen migration and metal ions play their roles on the radical capturing.

3.5 TGA curves of SR composites

The thermal stability of SR composites is reflected by TGA curves in Figure 6. And the corresponding characteristic data are listed in Table 5. All the samples underwent two steps of thermal oxidative degradation. The first one (weight loss ca. 10%) should be ascribed to the decomposition of low molecular mass additives and polyvinylsiloxane. In this step, a very significant feature is that the initial mass loss temperature of blank SR without heat resistant additive is at least about 30°C lower than those of SR composites, demonstrating the positive effect of modified stabilizer on the thermal oxidative degradation process of SR. And the second step is the main weight loss step which was chosen to compare the effect of additives on the thermal oxidative stability of SR. A temperature at weight loss of 50% (T_{50}) can reflect the thermal stability of SR composites. The addition of m-CeFeO-0.8 can significantly improve T_{50} from 541.7°C to 569.8°C, while the value for SR/m-CeO_2/Fe_2O_3 is just 557.7°C. Besides, SR/m-CeFeO-0.8 got the highest $T_{\text{Heat-resistance index}}$ (T_{HRI}) of 235.3°C among all the composites, indicating the prominent function of m-CeFeO-0.8 to improve the thermal oxidative stability of SR (27-29). The TGA results of SR composites are consistent with the mechanical properties results.

3.6 FTIR spectra of SR composites before and after aging

Figure 7 displays the FTIR spectra of SR composites which were applied to explore the status of the side groups before and after thermal oxidative aging. Two peaks stand out in the spectra at 1004 cm^{-1} and 784 cm^{-1} which could be ascribed to Si-O-Si and Si-CH_3. The intensity of the peak belongs to Si-O-Si group turn stronger after thermal oxidative aging while the intensity of the Si-CH_3 peak become weaker after aging, demonstrating that the destruction of side methyl and the formation of new Si-O-Si groups under the action of heat and oxygen. To further compare the effect of different CeFeO, the conservation rate (R) of the side methyl group were calculated as follows (30):

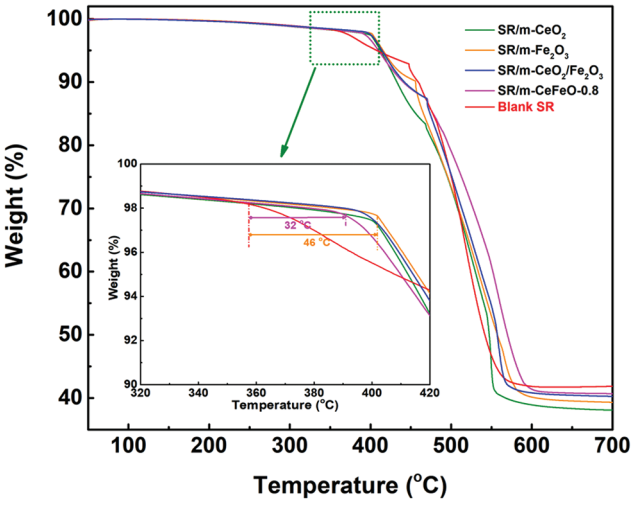

Figure 6: TGA curves of SR composites under air atmosphere.

Table 5: The characteristic data obtained from TGA curves (air, 20°C/min).

Sample	Weight loss temperature/°C			*T_{HRI}/°C	Residue/%
	T_5	T_{30}	T_{50}		
SR/m-CeO_2	412.6	508.0	547.0	230.2	38.3
SR/m-CeO_2/Fe_2O_3	413.7	511.3	557.7	231.4	40.3
SR/m-CeFeO-0.8	409.9	527.2	569.8	235.3	40.8
SR/m-CeFeO-0.6	405.8	516.8	560.9	231.4	40.7
SR/m-CeFeO-0.4	414.8	509.2	546.6	231.0	40.9
SR/m-CeFeO-0.2	413.6	510.8	547.9	231.2	40.3
SR/m-Fe_2O_3	415.6	509.2	557.4	231.2	39.3
Blank SR	408.0	508.8	541.7	229.5	42.3

*The sample's heat-resistance index is calculated by Eq. 2

$$T_{HRI} = 0.49 \times [T_5 + 0.6 \times (T_{30} - T_5)] \quad (2)$$

T_5 and T_{30} are the temperatures at weight losses of 5% and 30%, respectively.

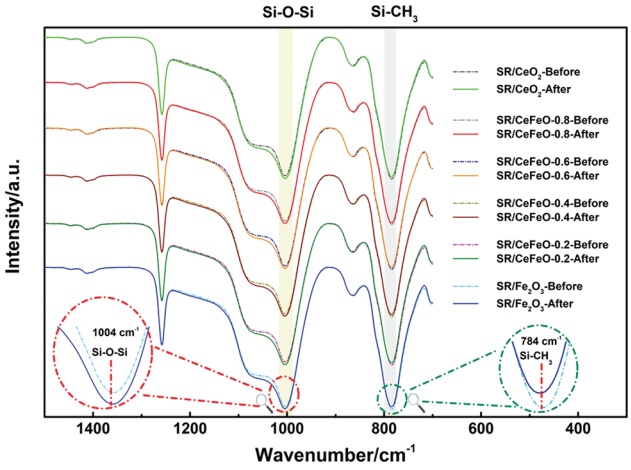

Figure 7: FTIR spectra of SR composites before and after thermal oxidative aging.

Table 6: The absorption intensity and conservation rate obtained from FTIR spectra.

Sample	Aging	$Abs_{Si\text{-}O\text{-}Si}$	$Abs_{Si\text{-}CH_3}$	R (%)
SR/m-CeO_2	Before	1.131	1.291	81.8
	After	1.242	1.160	
SR/m-CeFeO-0.8	Before	1.145	1.308	89.8
	After	1.215	1.207	
SR/m-CeFeO-0.6	Before	1.131	1.269	85.4
	After	1.223	1.172	
SR/m-CeFeO-0.4	Before	1.149	1.295	84.1
	After	1.237	1.173	
SR/m-CeFeO-0.2	Before	1.152	1.296	82.9
	After	1.237	1.154	
SR/m-Fe_2O_3	Before	1.151	1.299	82.2
	After	1.244	1.155	

$$\text{Conservation rate } (R) = \frac{Abs_{Si-CH_3}(\text{After aging}) \times Abs_{Si-O-Si}(\text{Before aging})}{Abs_{Si-O-Si}(\text{After aging}) \times Abs_{Si-CH_3}(\text{Before aging})} \quad (3)$$

where, $Abs_{Si\text{-}CH3}$ and $Abs_{Si\text{-}O\text{-}Si}$ are the absorption intensity of Si-CH_3 and Si-O-Si peaks, respectively, which can be calculated through the transmittance intensity (T):

$$Abs = -\lg T \quad (4)$$

The absorption intensity and R are listed in Table 6. After aging, R values of SR composites, especially SR/m-CeFeO-0.8, are higher than that of SR/m-CeO_2 and

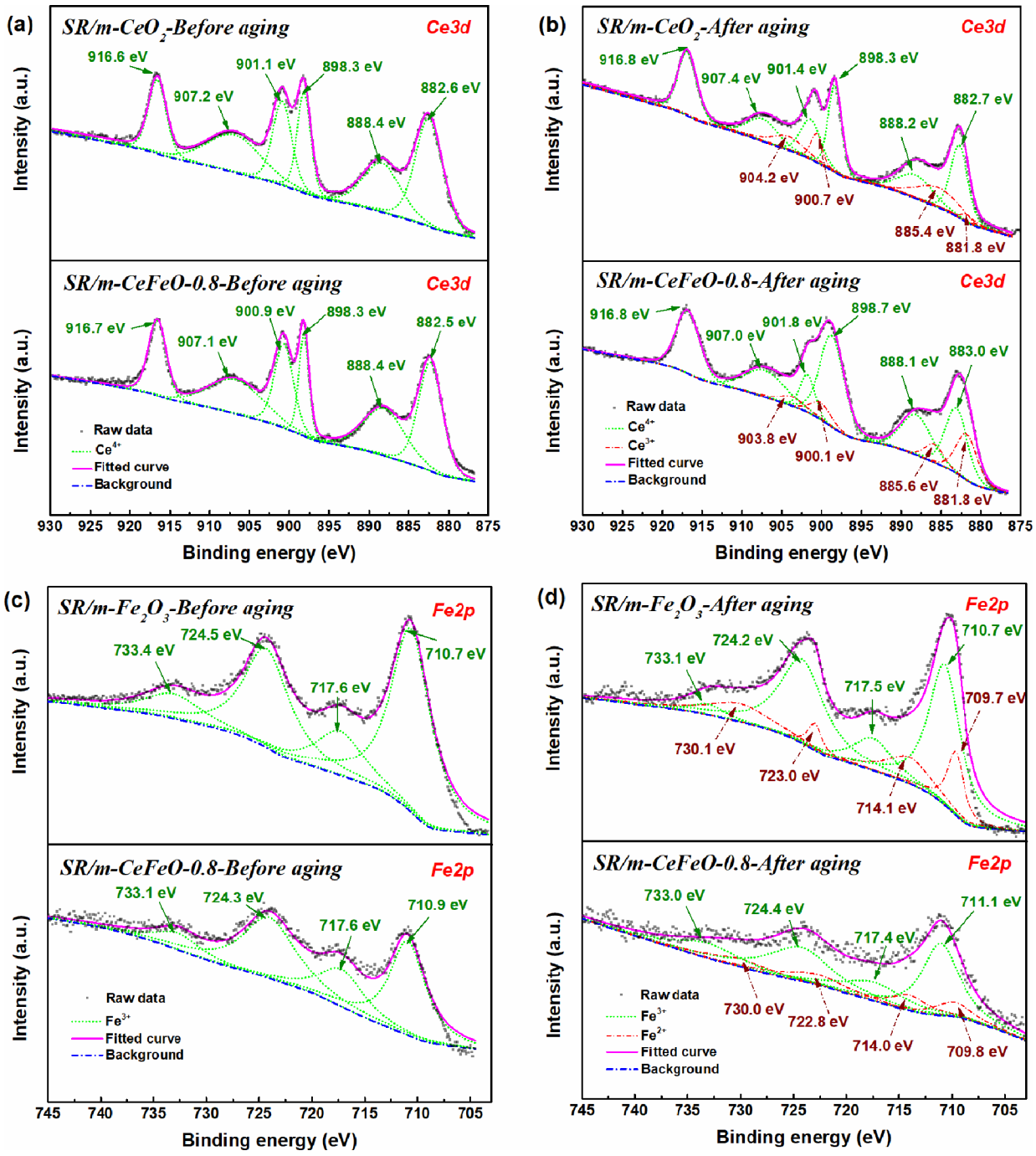

Figure 8: XPS spectra of Ce3d and Fe2p for SR composites before and after thermal oxidative aging: (a) Ce3d XPS spectra before aging; (b) Ce3d XPS spectra after aging; (c) Fe2p XPS spectra before aging; and (d) Fe2p XPS spectra after aging.

SR/m-Fe_2O_3, indicating that the combination of CeO_2 and Fe_2O_3 could effectively protect the side methyl groups from attacking by heat and oxygen.

3.7 XPS of SR compounds and composites

To study the radical capturing capability of metal oxides during the degradation process of silicone rubber, SR/m-CeO_2 (100/30), SR/m-Fe_2O_3 (100/30) and SR/m-CeFeO-0.8 (100/30) compounds were prepared and kept at an oven at 300°C for 48 h, and the aged and non-aged samples were characterized by XPS. The high-resolution XPS spectra of Ce3d and Fe2p for SR/m-CeO_2, SR/m-Fe_2O_3 and SR/m-CeFeO-0.8 compounds before after thermal oxidative aging are shown in Figure 8, and the characteristic data are listed in Table 7.

Table 7: The characteristic data of XPS spectra.

Samples	Binding energy (eV)	Peak area (%)
Aged SR/m-CeO_2 composite		
Ce^{4+}	$Ce3d_{5/2}$: 882.7 888.2 898.3 $Ce3d_{3/2}$: 901.4 907.4 916.8	77.8
Ce^{3+}	$Ce3d_{5/2}$: 881.8 885.4 $Ce3d_{3/2}$: 900.7 904.2	22.2
Aged SR/m-Fe_2O_3 composite		
Fe^{3+}	$Fe2p_{3/2}$: 710.7 717.5 $Fe2p_{1/2}$: 724.2 733.1	72.4
Fe^{2+}	$Fe2p_{3/2}$: 709.7 714.1 $Fe2p_{1/2}$: 723.0 730.1	27.6
Aged SR/m-CeFeO-0.8 composite		
Ce^{4+}	$Ce3d_{5/2}$: 883.0 888.1 898.7 $Ce3d_{3/2}$: 901.8 907.0 916.8	80.2
Ce^{3+}	$Ce3d_{5/2}$: 881.8 885.6 $Ce3d_{3/2}$:900.1 903.8	19.8
Fe^{3+}	$Fe2p_{3/2}$: 711.1 717.4 $Fe2p_{1/2}$: 724.4 733.0	75.3
Fe^{2+}	$Fe2p_{3/2}$: 709.8 714.0 $Fe2p_{1/2}$: 722.8 730.0	24.7

As shown in Figure 8a, there is no Ce^{3+} in non-aged SR/m-CeO_2 and SR/m-CeFeO-0.8 compounds. After aging, the SR compounds became vulcanizates, implying the occurrence of radical mechanism. In Figure 8b, the Ce3d XPS spectra retained the Ce^{4+} peaks ($3d_{5/2}$=882.7-883.0 eV, 888.1-888.2 eV and 898.3-898.7 eV; $3d_{3/2}$=901.4-901.8 eV, 907.0-907.4 eV and 916.8 eV). Moreover, the satellite peaks at 885.4-885.6 eV indicate the existence of Ce^{3+}. Besides, other peaks ($3d_{5/2}$=881.8 eV; $3d_{3/2}$=900.1-900.7 eV and 903.8-904.2 eV) are also associated with Ce^{3+} (21,31,32). The results indicated the partially conversion of Ce^{4+} to Ce^{3+} in aged SR composites. Similarly, Figure 8c shows there is no Fe^{2+} in non-aged SR/m-Fe_2O_3 and SR/m-CeFeO-0.8 compounds, while the Fe2p XPS spectra in Figure 8d show the co-existence of Fe^{3+} and Fe^{2+} in aged samples (33,34). As shown in Table 7, the aged SR/m-CeFeO-0.8 composite got a $Fe^{3+}/(Fe^{3+}+Fe^{2+})$ ratio of 75.3% and a $Fe^{2+}/(Fe^{3+}+Fe^{2+})$ ratio of 24.7%, while the contents of $Ce^{4+}/(Ce^{4+}+Ce^{3+})$ and $Ce^{3+}/(Ce^{4+}+Ce^{3+})$ in the aged SR/m-CeFeO-0.8 composite are about 80.2% and 19.8%, respectively. The results indicate that Fe^{3+} behaves very active in radical quenching. Moreover, compared with SR/m-CeO_2 and SR/m-Fe_2O_3, SR/m-CeFeO-0.8 composite has less ratios of $Fe^{2+}/(Fe^{3+}+Fe^{2+})$ and $Ce^{3+}/(Ce^{4+}+Ce^{3+})$ after aging. Previous studies in the field of catalysis confirm that the incorporation of low-state Fe^{3+} into CeO_2 lattice could facilitate the migration of oxygen, leading to a fast re-oxidation of Fe^{2+} and Ce^{3+}, then a redox cycle is formed. Therefore, the synergistic effect of CeO_2 and Fe_2O_3 in CeFeO on the thermal oxidative stability of silicone rubber may be related to the fast redox cycle occurred in CeFeO to enable the continuity of free-radical quenching.

4 Conclusion

Ce-Fe complex oxides were successfully synthesized. A Ce-Fe complex oxide with Ce/(Ce+Fe) molar ratio of 0.8 (CeFeO-0.8) could significantly improve the thermal oxidative stability of silicone rubber. After aging at 300°C for 24 h, silicone rubber filled with 4 phr CeFeO-0.8 has higher retentions of tensile strength and elongation at break, smaller changing amplitude of crosslink density and lower conversion rate of the side methyl group compared with silicone rubbers filled pure CeO_2 and Fe_2O_3. Ce^{4+} and Fe^{3+} could react with radicals produced in the thermal degradation process of silicone rubber and the Ce and Fe in Ce-Fe complex oxide have positive synergistic effect on radical capturing as confirmed by XPS spectra. These results indicate that Ce-Fe complex oxides has good potential applications in the manufacture of heat resistant silicone rubber.

Acknowledgements: This work is supported by National Natural Science Foundation of China (No. 51273109).

References

1. Patel M., Skinner A.R., Thermal ageing studies on room-temperature vulcanized polysiloxane rubbers. Polym Degrad Stab, 2001, 73(3), 399-402.
2. Camino G., Lomakin S.M., Lazzari M., Polydimethylsiloxane thermal degradation, Part 1. Kinetic aspects. Polymer, 2001, 42(6), 2395-2402.
3. Camino G., Lomakin S.M., Legeard M., Thermal polydimethylsiloxane degradation Part 2. The degradation mechanisms. Polymer, 2002, 43(7), 2011-2015.
4. Thomas T.H., Kendrick T.C., Thermal analysis of polysiloxanes. II. Thermal vacuum degradation of polysiloxanes with different substituents on silicon and in the main siloxane chain. J Polym Sci, Part A: Polym Chem, 1970, 8, 1823-1830.
5. Warrick E.L., Pierce O.R., Polmanteer K.E., Saam J.C., Silicone Elastomer Developments 1967-1977. Rubber Chem Technol, 1979, 52(3), 437-525.
6. Hayashida O., Kazuhiro O., Atsuhito K., Silicone Rubber Composition Having Excellent Heat Resistance. 2015, EP2554585 B1.
7. Katusic S., Michael G.D., Miess H., Scholz M., Kunzmann K., Albers P., Pyrogenically-produced cerium oxide useful in polishing sensitive electronics surfaces, as a heat stabilizer for silicone rubber or as a catalyst has specified coarse and fine fractions. 2004, DE10251029 A1.

8. Fei H.F., Han X.J., Liu B.Z., Gao X.Y., Wang Q., Zhang Z.J., et al., Mechanism of the antioxidation effect of α-Fe_2O_3 on silicone rubbers at high temperature. RSC Adv, 2016, 6(10), 7717-7722.
9. Li H.Y., Tao S., Huang Y.H., Su Z.T., Zheng J.P., The improved thermal oxidative stability of silicone rubber by using iron oxide and carbon nanotubes as thermal resistant additives. Compos Sci Technol, 2013, 76, 52-60.
10. Zhang X., Zhang Q., Zheng J.P., Effect and mechanism of iron oxide modified carbon nanotubes on thermal oxidative stability of silicone rubber. Compos Sci Technol, 2014, 99, 1-7.
11. Bai L., Bai Y.L., Zheng J.P., Improving the filler dispersion and performance of silicone rubber/multi-walled carbon nanotube composites by noncovalent functionalization of polymethylphenylsiloxane. J Mater Sci, 2017, 52(12), 7516-7529.
12. Bai L., Wang X., Tan J., Li H.Y., Zheng J.P., Study of distinctions in the synergistic effects between carbon nanotubes and different metal oxide nanoparticles on enhancing thermal oxidative stability of silicone rubber. J Mater Sci, 2016, 51(15), 7130-7144.
13. Wu Y.L., Bai Y.L., Zheng J.P., Effects of Polyhedral Oligomeric Silsesquioxane Functionalized Multi-walled Carbon Nanotubes on Thermal Oxidative Stability of Silicone Rubber. Sci Adv Mater, 2014, 6(6), 1244-1254.
14. Qiu X.N., Cai H., Fang X., Zheng J.P., The improved thermal oxidative stability of silicone rubber by incorporating reduced graphene oxide: Impact factors and action mechanism. Polym Compos, 2018, 39(4), 1105-1115.
15. Chen D.Z., Yi S.P., Wu W.B., Zhong Y.L., Liao J., Huang C., et al., Synthesis and characterization of novel room temperature vulcanized (RTV) silicone rubbers using Vinyl-POSS derivatives as crosslinking agents. Polymer, 2010, 51(17), 3867-3878.
16. Liu Y.F., Shi Y.H., Zhang D., Li J.L., Huang G.S., Preparation and thermal degradation behavior of room temperature vulcanized silicone rubber-g-polyhedral oligomeric silsesquioxanes. Polymer, 2013, 54(22), 6140-6149.
17. Bai L., Zheng J., Synergistic effect of iron oxide modified carbon nanotubes on the thermal stability of silicone rubber under different atmospheres. J Therm Anal Calorim, 2016, 123(2), 1281-1291.
18. Liang C., Ma Z., Lin H., Ding L., Qiu J., Frandsen W., Su D., Template preparation of nanoscale $Ce_xFe_{1-x}O_2$ solid solutions and their catalytic properties for ethanol steam reforming. J Mater Chem, 2009, 19(10), 1417-1424.
19. Li K., Wang H., Wei Y., Yan D., Direct conversion of methane to synthesis gas using lattice oxygen of CeO_2-Fe_2O_3 complex oxides. Chem Eng J, 2010, 156(3), 512-518.
20. Bao H., Chen X., Fang J., Jiang Z., Huang W., Structure-activity relation of Fe_2O_3-CeO_2 composite catalysts in CO oxidation. Catal Lett, 2008, 125(1-2), 160-167.
21. Rocha M.A.L., Ángel G.D., Torres-Torres G., Cervante A., Vázquez A., Arrieta A., et al., Effect of the Pt oxidation state and Ce^{3+}/Ce^{4+}, ratio on the Pt/TiO_2-CeO_2, catalysts in the phenol degradation by catalytic wet air oxidation (CWAO). Catal Today, 2015, 250, 145-154.
22. Kuang W., Fan Y., Yao K., Chen Y., Preparation and Characterization of Ultrafine Rare Earth Molybdenum Complex Oxide Particles. J Solid State Chem, 1998,140(2), 354-360.
23. Cornell R.M., Schwertmann U., The iron oxides: structure, properties, reactions, occurrence and uses. Mineral Mag, 1997, 61(5), 740-741.
24. Elias J.S., Risch M., Giordano L., Mansour A.N., Shao-Hom Y., Structure, Bonding, and Catalytic Activity of Monodisperse, Transition-Metal-Substituted CeO_2 Nanoparticles. J Am Chemi Soc, 2014, 136(49), 17193-17200.
25. Zhang Z., Han D., Wei S., Zhang Y., Determination of active site densities and mechanisms for soot combustion with O_2, on Fe-doped CeO_2, mixed oxides. J Catal, 2010, 276(1), 16-23.
26. Mcbride J.R., Hass K.C., Poindexter B.D., Weber W.H., Raman and x-ray studies of $Ce_{1-x}RE_xO_{2-y}$, where RE=La, Pr, Nd, Eu, Gd, and Tb. J Appl Phys, 1998, 76(4), 2435-2441.
27. Gu J.W., Meng X.D., Tang Y.S., Yang L., Zhuang Q., Kong J., Hexagonal boron nitride/silicone rubber dielectric thermally conductive composites with excellent thermal stabilities. Compos Part A-Appl S, 2017, 92, 27-32.
28. Gu J.W., Lv Z.Y., Wu Y.L., Guo Y.Q., Tian L.D., Qiu H., et al., Dielectric thermally conductive boron nitride/polyimide composites with outstanding thermal stabilities via in-situ polymerization-electrospinning-hot press method. Compos Part A-Appl S, 2017, 94, 209-216.
29. Gu J., Dong W., Xu S., Tang Y., Ye L., Kong J., Development of wave-transparent, light-weight composites combined with superior dielectric performance and desirable thermal stabilities. Compos Sci Technol, 2017, 144, 185-192.
30. Qiu J., Lai X., Li H., Zeng X., Zhang Z., Synthesis of Zirconium-Containing Polyhedral Oligometallasilsesquioxane as an Efficient Thermal Stabilizer for Silicone Rubber. Polymers, 2018, 10(5), 520.
31. Katta L., Kumar T.V., Durgasri D.N., Reddy B.M., Nanosized $Ce_{1-x}La_xO_{2-\delta}/Al_2O_3$ solid solutions for CO oxidation: Combined study of structural characteristics and catalytic evaluation. Catal Today, 2012, 198(1), 133-139.
32. Lin T.N., Lee M.C., Yang R.J., Chang J.C., Kao W.X., Lee L.S., Chemical state identification of Ce^{3+}/Ce^{4+}, in the $Sm_{0.2}Ce_{0.8}O_{2-\delta}$, electrolyte for an anode-supported solid oxide fuel cell after long-term operation. Mater Lett. 2012, 81, 185-188.
33. Aronniemi M., Sainio J., Lahtinen J., Chemical state quantification of iron and chromium oxides using XPS: the effect of the background subtraction method. Surf Sci, 2005, 578(1-3), 108-123.
34. Roosendaal S.J., Asselen B.V., Elsenaar J.W., Vredenberg A.M., Habraken F.H.P.M., The oxidation state of Fe(100) after initial oxidation in O_2. Surf Sci, 1999, 442(3), 329-337.